Adaptive differential protection scheme for wind farm integrated power network

Ch. Durga Prasad[a], Monalisa Biswal[a], Almoataz Y. Abdelaziz[b],[*]

[a] Department of Electrical Engineering National Institute of Technology, Raipur 492010, India-
[b] Faculty of Engineering and Technology, Future University in Egypt, Cairo 11835, Egypt

ABSTRACT

In this paper, an adaptive differential protection scheme is proposed for wind farm integrated power network. Any fixed threshold setting based protection scheme is not always suitable for the different operating conditions of power system. Considering the possible modulations in the fault signal, a particle swarm optimization (PSO) based differential relay algorithm is proposed in this paper. The positive sequence current differential principle is used. For different operating conditions, fault conditions and configurations of the system, the threshold value can be calculated online. So, practically the method can be applied to any power system model and the impact of dynamic operation of wind farm on the protection function is negligible. The threshold setting is designed considering the fault location and fault inception angle. Initially, the most effective faults among all the possible faults are identified with a single variable (fault location) objective function. Later, only single-phase-to-ground fault is considered for threshold setting with all possible parameters. The method is tested using a standard power system model integrated with wind farm and simulated using MATLAB R2016a software. Results prove the efficacy of the method.

1. Introduction

Integration of large-scale renewable sources into existing power system is increasing in recent years in view of reducing large carbon emission and encouraging more utilization of green technologies [1]. As the natural resources are plently available with free of cost, bulk amount of power generation from these sources are encouraged day-by-day. On the other hand, the problem that arises due to the integration of wind farm is the variable wind speed [2–5]. The variation in operating conditions of wind farm (WF) leading to power, frequency and voltage fluctuations may create new challenges for existing protection algorithms. The conventional line protection schemes are based on prefixed settings and practically not suitable for dynamic operating conditions of the system [6,7]. To mitigate this issue, adaptive distance protection schemes were proposed [7–11] considering the variations of large-scale wind farms. The effect of variations in wind-farm parameters on the reach setting is extensively studied and an adaptive protection scheme for distribution and transmission lines including WF is proposed in [11]. The procedure of distance relay setting is complex in the presence of wind farm and the reliability of relaying function is poor in case of remote end and high impedance faults [12]. Hence differential relaying schemes [13–17] are applied for transmission line protection in

presence of wind farms. The advancement in communication technologies helps in developing more reliable differential relay schemes for transmission network including WF [12]. But the performance of current differential scheme presented in [13] is get affected by the presence of DFIG. Further, threshold setting is a challenging task due to dynamic operations of wind farms. Later power and energy differential schemes were developed and reported in [14–16]. Such differential schemes generally malfunction under large power fluctuation conditions initiated due to random change in the wind speed [17]. Under the same scenario, the performance of Hilbert transform and Teager Energy based differential scheme [18] is also not reliable. By considering the existing drawbacks of aforementioned conventional techniques, new strategies were proposed in [17,19]. But higher computational burden and requirement of large training data are the major drawbacks of these techniques. Considering the above-mentioned challenges, an adaptive swarm intelligence-based threshold selection procedure is proposed to the positive sequence current differential protection algorithm for overhead lines. The adaptive threshold selection process enhances the functionality of differential protection and hence guarantees the system security during fault conditions. The proposed algorithm is tested for several operating conditions including variations in wind speed, and different fault cases. The impact of sampling frequency on the

[*] Corresponding author.
E-mail addresses: dpchinta@srkrec.edu.in (C.D. Prasad), almoatazabdelaziz@hotmail.com, almoataz.abdelaziz@fue.edu.eg (A.Y. Abdelaziz).
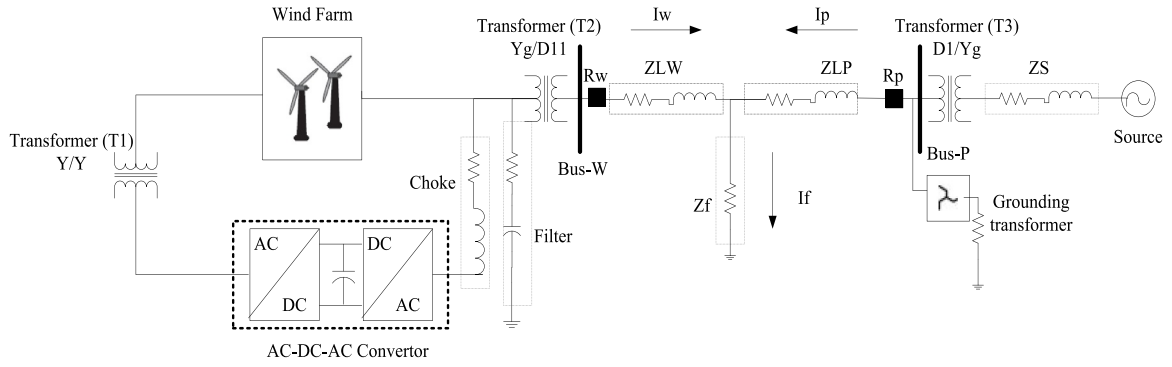
Fig. 1. Studied power system.

performance of proposed method is also tested. A standard power network model integrated with wind farm is considered for analysis and simulated using MATLAB R2016a software.

2. Power system model

The wind farm integrated power system model shown in Fig. 1 is considered for analysis and verification of the adaptive threshold based differential protection scheme. The line connected between buses W and P is of 30 km. Wind turbines of capacity 9 MW (6*1.5 MW) are connected on bus-W through a step-up transformer. The doubly-fed induction generator (DFIG) based wind turbines consists of a wound rotor induction generator with rotor side resistance of 0.016 p.u. and reactance of 0.16 p.u. On stator side, the winding resistance and re-actance are 0.023 p.u and 0.18 p.u. The system frequency is 60 Hz. The stator winding is connected to the grid directly while the rotor is con-nected through the AC/DC/AC IGBT-based pulse width modulation (PWM) converter. In order to achieve desired accuracy, rotor side PWM carrier frequency is set at 1620 Hz for the AC/DC/AC IGBT-based back to back converter, and grid-side PWM carrier frequency is set at 2700 Hz. Other system parameters along with the specifications of individual components are provided in the Appendix [20]. The signals are ex-tracted with a sampling frequency of 1.2 kHz to implement the pro-posed swarm assisted adaptive differential protection scheme. Model-ling and simulation work are done using sim-powersystem toolbox and algorithm is tested using MATLAB R2016a software.

3. Proposed method

In the proposed scheme, the current at buses W and P are measured and the measurement from bus-W side is communicated to bus-P to estimate the differential positive sequence current. At relay (R_p) end all the computational work is performed. For any fault in the line between buses W and P, the equivalent positive sequence network diagram for the studied system (Fig. 1) is shown below in Fig. 2. E_{AW1} and E_{AP1} are the positive sequence voltages of both the sources behind buses W and P. The source impedances are Z_{SW1} and Z_{SP1}.

I_W and I_P are the positive sequence currents measured at bus W and bus P during fault. By applying Kirchhoff's voltage law (KVL) to the loop-1 (wind farm side) of Fig. 2, Eq. (1) can be obtained as follows:
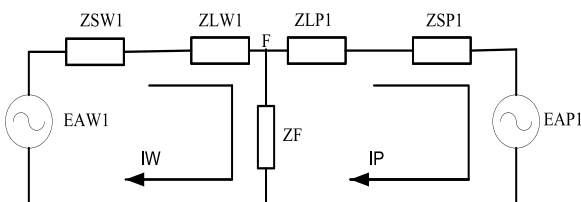
Fig. 2. Positive sequence network during fault condition.

$$E_{AW1} - I_W(Z_{SW1} + Z_{LW1} + Z_F) + I_P Z_F = 0 \tag{1}$$

By taking, $Z_{SW1} + Z_{LW1} + Z_F = Z'_x$, further Eq. (1) can be modified as

$$E_{AW1} - I_W Z'_x + I_P Z_F = 0 \tag{2}$$

Similarly, for loop-2 the KVL equation will be

$$-I_P Z''_x - E_{AP1} + I_W Z_F = 0 \tag{3}$$

Considering $Z''_x = Z_{SP1} + Z_{LP1} + Z_F$, Eq. (3) can be rearranged as

$$I_W = \frac{I_P Z''_x + E_{AP1}}{Z_F} \tag{4}$$

Substituting (4) in (2), we get

$$I_P = \frac{E_{AW1}}{a} - \frac{E_{AP1}a_1}{a} \tag{5}$$

where $a = \frac{Z'_x Z''_x - Z_F^2}{Z_F}$ and $a_1 = \frac{Z'_x}{Z_F}$. The current I_w can rearranged as

$$I_W = \frac{\left(\frac{E_{AW1}}{a} - \frac{E_{AP1}a_1}{a}\right)Z''_x + E_{AP1}}{Z_F} \tag{6}$$

By using Eqs. (5) and (6), the differential positive sequence current during fault condition can be calculated as

$$|I_P - I_W| = \left|\left(\frac{E_{AW1}}{a} - \frac{E_{AP1}a_1}{a}\right)a_2 - E_{AP1}a_3\right| \tag{7}$$

where $a_2 = 1 - \frac{Z''_x}{Z_F}$ and $a_3 = \frac{1}{Z_F}$. By using Eq. (7), a fault condition can be registered only when

$$|I_P - I_W| > \vartheta \tag{8}$$

Hence for the reliable detection of fault condition within the pro-tected section, selection of proper threshold is imperative. So, the op-erating quantity of Eq. (8) is a function of (a, a_1, a_2) and can be written as

$$|I_P - I_W| = \left|\left(\frac{E_{AW1}}{a} - \frac{E_{AP1}a_1}{a}\right)a_2 - E_{AP1}a_3\right| = \psi(a, a_1, a_2) \tag{9}$$

In Eq. (9), E_{AW1} and E_{AP1} are constants and hence the function de-pends on the values of a, a_1, and a_2. Further, the values of a, a_1, and a_2 depend on the fault location, fault impedance and fault inception time. In this work the fault location (x) and fault inception time (t_s) are considered as operating variables for the generation of suitable threshold for the system. So, by considering the variables x and t_s, the Eq. (9) can be further expressed as:

$$|I_P - I_W| = \psi(a, a_1, a_2) = g(x, t_s) \tag{10}$$

The minimum value obtained from the function considering two operating variables is selected as a threshold for the differential algo-rithm. Out of the two variables, the magnitude of fault detection index (FDI) varies significantly with respect to x. Hence, to obtain the optimal threshold with respect to 'x' the objective function of the problem can

be formulated by considering all 11-types of faults (AG, BG, CG, AB, BC, AC, ABG, BCG, ACG, ABC, ABCG). The optimal threshold can be obtained as

$$\vartheta = \min \begin{Bmatrix} g_{AG}(x), g_{BG}(x), g_{CG}(x), g_{AB}(x), g_{BC}(x), g_{CA}(x), \\ g_{ABG}(x), g_{BCG}(x), g_{ACG}(x), g_{ABC}(x), g_{ABCG}(x) \end{Bmatrix} \quad (11)$$

For the above objective function, the boundary values of fault location (x) lies in between 0 to L.

$$0 \le x \le L \quad (12)$$

where, L is the total length of the line in km. Instead of considering the extreme line length limits, a small deviation (ξ) in both upper and lower limit is applied. So, the fault location can be varied in between ξ and L-ξ as mentioned in Eq. (13).

$$\xi \le x \le L - \xi \quad (13)$$

The threshold setting problem is extended as a multi dimensional problem. Out of the different sub-functions, few sub-functions are less influential and thus can be ignored. Fault involving more than one phase is negelected and only single-phase-to-ground faults (LG) are considered as a function to generate the reliable threshold. Considering the LG faults, the modified objective function can be written as [24–25].

$$\vartheta = \min \{ g_{AG}(x, t_s), g_{BG}(x, t_s), g_{CG}(x, t_s), \} \quad (14)$$

Along with the variable ′x′, ′t_s′ is also considered to convert the single dimensional problem into two-dimensional problem. So, the time constraint included in the new objective function can be written as

$$t_{\min} \le t_s \le t_{\max} \quad (15)$$

In Eq. (15), $t_{\min}$ and $t_{\max}$ are the minimum and maximum limits of fault initiation time expressed in seconds. The maximum and minimum time limits should be selected in such a manner that the difference between the maximum to minimum value is equal to exactly one cycle time period i.e. 0.02 sec for 50 Hz and 0.0167 for 60 Hz. For each objective function, subjected to corresponding constraints, the optimal threshold value can be achieved by using any swarm intelligent optimization technique. In this work, particle swarm optimization (PSO) is used for this purpose. For random values of x and t_s, different FDI can be computed using for the differential positive sequence current using Eq. (10). But the minimum FDI cannot be achieved by hit and trail method. So, PSO technique is applied to achieve an optimal threshold value. The applications of PSO technique in solving many engineering problems are reported in [21–23]. PSO provides an optimum solution in case where the threshold selection is a very complex task. Even with complex problem, reliable and desired solution can be obtained using PSO technique. In the initial iterative stage, the position of every individual swarm is p_i^k and the velocity is v_i^k. The best position of each organism is p_{best} and the overall optimized best among all particles is g_{best}. The velocity is updated by comparing the previous and the new fitness values and accordingly the position of the swarm can be updated. The velocity and position of each particle can be updated using (16) and (17)

$$v_i^{k+1} = \omega v_i^k + c_1 r_1 \left(p_{best_i} - p_i^k \right) + c_2 r_2 \left(g_{best_i} - p_i^k \right) \quad (16)$$

$$p_i^{k+1} = p_i^k + v_i^{k+1} \quad (17)$$

In Eq. (16), c_1 and c_2 are acceleration constants, r_1 and r_1 are random numbers varies from 0 to 1. ω is the inertia weight factor. As mentioned in [22], several variants of PSO are proposed later after conventional PSO to avoid pre-maturity caused by selection of control parameters. The selection of inertia weight is complex [23] and several mechanisms are available for its selection. To avoid pre-maturity condition of PSO, the inertia weight factor can be set using (18)

$$\omega^{k+1} = \omega^k * \omega_{damp} \quad (18)$$

In Eq. (18), ω_{damp} is the damping ratio of inertia weight. Depending on the common parameters of PSO i.e. population number and iteration number, extensive cases are simulated within the boundaries of the variables for every iteration. However, the effectiveness of Eq. (18) on threshold selection process is discussed in details in Section 6.

4. Simulation results

For the considered test system (Fig. 1), the optimal FDI can be obtained by solving two stage problem. Stage-1 is a single variable problem in which x is varying and t_s is treated as constant. But stage-2 is considered as a multi-variable problem.

4.1. Stage-1:Threshold setting using single variable objective function

In this process, the objective function mentioned in Eq. (11) involves all sub-functions including the different possible faults. For optimization of each sub-function, 50 iterations are considered with population size of 100. For the given test system shown in Fig. 1, the first constraint x is considered to be a variable and expressed as

$$1 \le x \le 29 \quad (19)$$

However, t_s is taken as constant. After identifying the individual optimal indices for all possible faults that occurred for the simulated system, the overall unique optimum threshold index can be fixed by using Eq. (11). The obtained optimal indices for all fault cases are mentioned in (20)

$$\vartheta = \min \begin{Bmatrix} 0.6113, 0.5035, 0.3915, 2.1619, 2.1561, \\ 2.1566, 2.3394, 2.3208, 2.3261, 4.6245 \end{Bmatrix} = 0.3915 \quad (20)$$

The optimal threshold is obtained for CG fault and fault location 23.1587 km from bus-P. For the different types of fault, the optimal FDI along with the critical fault locations are estimated using the proposed method and presented in Table 1. For ABC and ABCG faults the same optimal indices are achieved.

The solution obtained from stage-1 is enough to set optimal threshold under normal operating condition. Fig. 3 shows the process of identification of optimal index from initial iteration to final iteration for all the possible LG faults. The optimal value obtained from a single variable used in stage-I and shown in Fig. 4(a) and corresponding FDI are shown in Fig. 4(b). The main advantage of applying swarm intelligence technique in threshold section procedure can be clearly observed from Fig. 3 and Fig. 4.

By applying conventional methods, the threshold value can be selected using regular trial and error method. But from Fig. 3, it can be understood that due to large variations in threshold value during LG fault, in between 10 to 30 km fault location, such a trial and error process is not suitable. But the proposed threshold searching method using PSO technique is able to identify optimal value of ϑ within minimum number of iterations and the obtained solutions are reliable as evident from Fig. 4(a) and Fig. 4(b). The surfaces generated from PSO show the importance of application of swarm intelligence to optimal threshold setting problem.

However, stage-2 is employed to generate more reliable detection index by including fault inception time which is discussed below.

Table 1
Optimal indices obtained for different faults with $t_s = 0.4$ sec and fault resistance $= 1\Omega$.

Fault Type	Location (km)	FDI	Fault Type	Location (km)	FDI
AG	28.8205	0.6113	AC	28.8631	2.1566
BG	28.8247	0.5035	ABG	28.8955	2.3394
CG	23.1587	0.3915	BCG	28.9696	2.3208
AB	29.0000	2.1619	ACG	29.0000	2.3261
BC	28.7340	2.1561	ABC	28.8924	4.6245
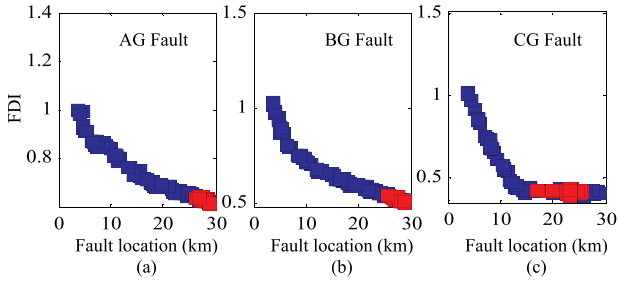
Fig. 3. Optimal threshold searching pattern using PSO for LG faults using stage-1.
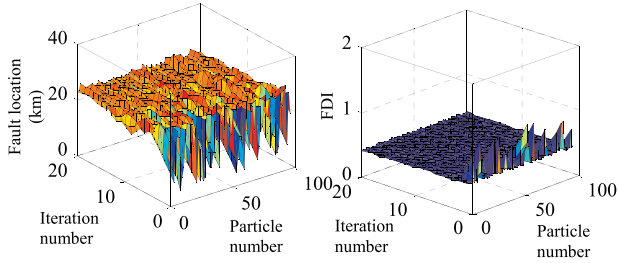
Fig. 4. Surfaces generated by PSO in the search process of AG fault under stage-1.

4.2. Stage-2: Threshold setting using multi variable objective function

Out of the 11 sub-functions in the main objective function, only three sub-functions corresponding to LG faults (AG, BG and CG) having minimum threshold indices, hence for stage-2 the objective function is mentioned Eq. (14). Along with the constraint mentioned in Eq. (19), the following constraint is included for the initiation of fault.

$$0.4 \leq t_s \leq 0.42 \tag{21}$$

Test system presented in this paper is operating at frequency of 60 Hz. But for 50 Hz operating system, a time margin of 0.02 sec is allocated to fault initiation for adapting the optimal value. Using the proposed approach with all constraints are taken into consideration, the FDI generated by PSO for all LG faults from the initial iteration to final iteration is presented in Fig 5. The total surface generated by PSO for a CG fault is presented in Fig. 6.

By using PSO, the optimal solution is achieved at 18.9150 km from bus-P with a fault initiation time of 0.4044 sec for AG fault. The fault resistance corresponding to optimal index is fixed and considered as 1Ω in the entire simulation studies in the stages of optimal threshold selection procedure. Table 2 shows the critical values of fault location, fault inception time for all the LG faults. Finally, the optimal index considered as a threshold for the given test system is obtained as 0.3137. Similar to stage-1, surfaces of variables generated by PSO are presented in Fig. 7 to show the strength of swarm intelligence application in this paper.

In Fig. 8, the obtained optimal threshold values for different LG
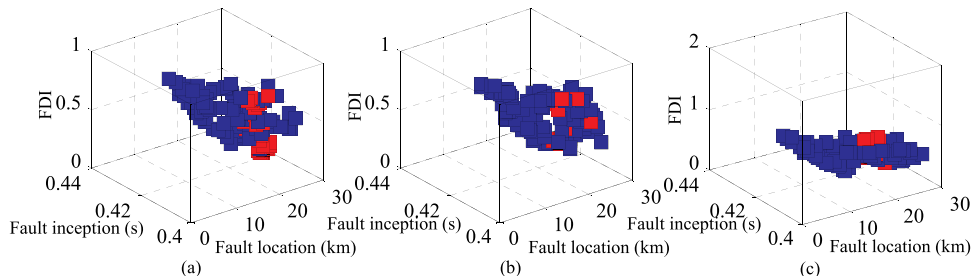
faults are plotted. Further the performance analysis of proposed method is tested for random faults as illustrated in the following case studies.

4.3. Response for LG Faults

The proposed optimal threshold searching process using two objective functions mentioned in Eqs. (11) and (14) are tested for different possible cases simulated for LG faults. A total of 5 trails are executed with a population size of 100. For each trail, 50 iterations are considered. Therefore, for two objective functions, 150000 LG faults are simulated as per Eq. (22).

total number of simulations in LG fault case

$$= (type\ of\ LG\ faults)*(no.\ of\ objective\ functions)$$
$$*(no.\ of\ trails)*(population\ size)*(number\ of\ iterations) \tag{22}$$

Few cases are simulated to check the proposed threshold setting mechanism applied to differential protection scheme. For AG fault initiated at 0.4 sec and 18 km from bus P, the obtained results are shown in Fig. 9(a). Fig. 9(b) shows the response for CG fault created at 24 km from bus P with a fault initiation time of 0.6 sec. for both the cases, fault resistance is 30 Ω. The FDI is more for AG fault case as compared to CG fault. But still the optimal threshold is reliable can able to detect the fault using differential principle. In both cases, trip signal is generated between 2-5 msec.

4.4. Response for double-line (LL and LLG) Faults

For the multi variable objective function in stage-2, double-phase and symmetrical faults are not considered during optimal threshold selection process because the FDI generated during such faults are more than LG faults. Hence only 75000 simulation cases are tested in stage-1 using PSO. However, few case studies are investigated to show the effectiveness of the proposed method. In this case, BC fault with a fault resistance of 5Ω, fault distance of 10 km from bus P and fault initiation time of 0.55 sec is considered. Fig. 10 (a) shows the results for the BC fault case. From Fig. 10(a), the trip signal in generated after 3 msec. Fig. 10(b) shows the performance of the proposed method for ACG fault with a fault distance of 28 km from bus P, fault time and fault resistance are 0.42 sec. and 40Ω respectively. By the optimal threshold value, the fault during ACG fault is detected just after 3 ms of fault initiation.

4.5. Response for symmetrical faults

For symmetrical faults, 5000 simulation cases are tested during optimal threshold setting procedure. For symmetrical faults, indices are larger than other faults. For an ABC fault with 5Ω fault resistance, 20 km fault distance from bus P and 0.5 sec fault initiation time, response of the method is shown in Fig. 11(a). In Fig. 11 (b) result for ABCG fault t_s is 0.3 sec, fault resistance 20Ω and *x is* 15 km from bus P. The fault is detected after 4 ms of fault initiation in both the ABC and ABCG fault cases.

Fig. 5. Variation of threshold from initial iteration to final iteration for stage 2 of AG fault.
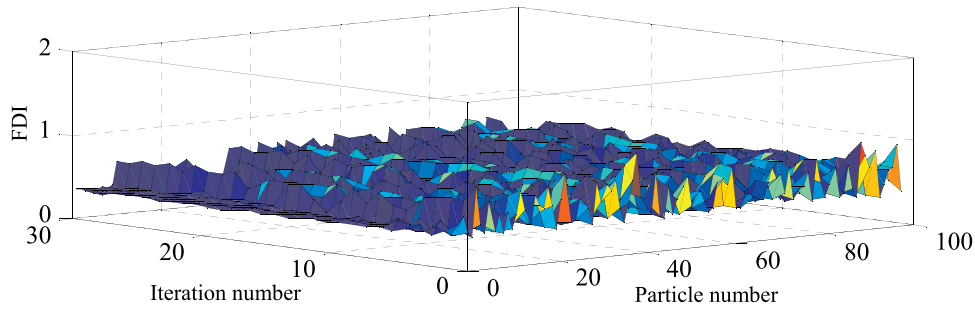
Fig. 6. FDI generated by PSO for CG fault in case of stage-2.

Table 2
Optimal indices obtained for LG faults using stage-2, fault resistance = 1Ω.

Fault	Location (km)	Inception (sec)	FDI
AG	18.9150	0.4044	0.3137
BG	18.9863	0.4102	0.3228
CG	20.9928	0.4155	0.3203

4.6. Response during varying fault location and inception time

In the first case, the fault resistance and inception time are considered as 10Ω and 0.3 sec. The FDI at various locations of the line for AG, AB, ABG and ABCG fault cases are simulated. A total of 120 cases are investigated and results are shown in Fig. 12. The results for unsymmetrical faults are shown in Fig. 12(a) and in Fig. 12(b) the FDI for ABCG fault case is provided. The optimal threshold for the studied test system is obtained as 0.3137. For all the fault cases, the calculated indices are lie consistently above the threshold. Next, the values of both fault location and inception time are varied. The value of t_s is varied
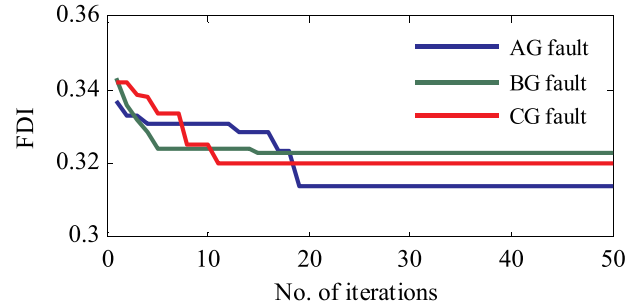
Fig. 8. FDI plots for single-line-to-ground faults.

from 0.2 to 0.6 and two fault cases are tested. Fault resistance is 10Ω. For BG and ABCG fault cases results are shown in Fig. 13. A total of 40 cases are tested. From the analysis it is understood that through the optimal threshold value reliable detection of fault under varying fault location and inception time is possible.
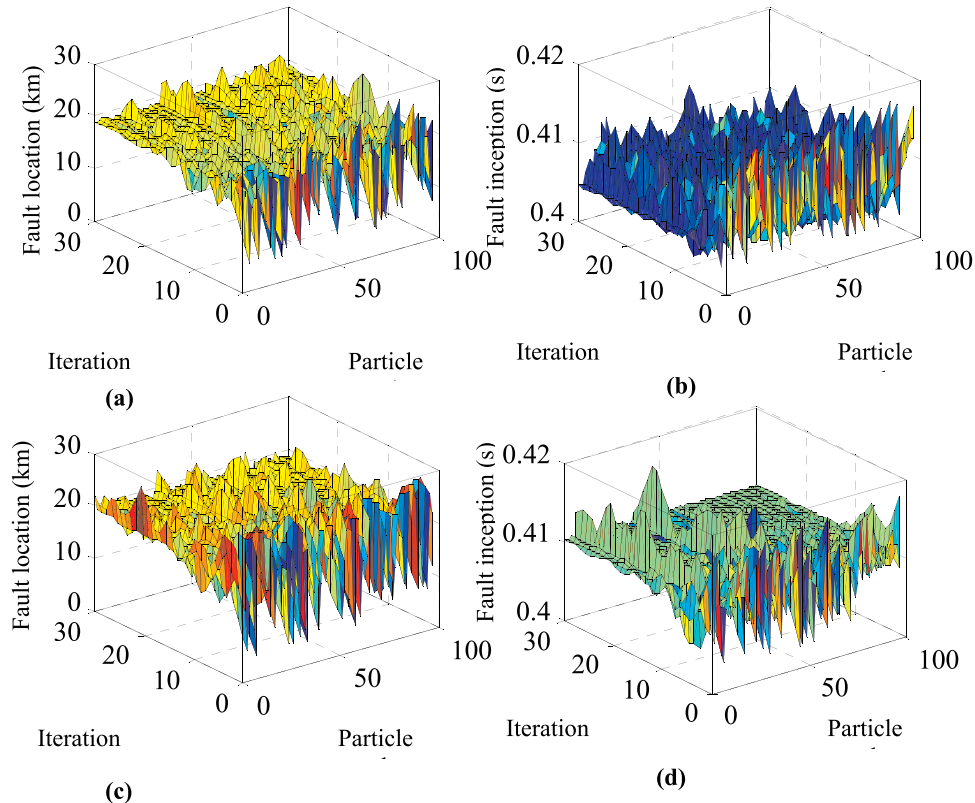
Fig. 7. Pattern of variations of (a) Location for AG fault. (b) Inception for AG fault. (c) Location for BG fault. (d) Inception for BG fault from initial to final iterations by PSO.
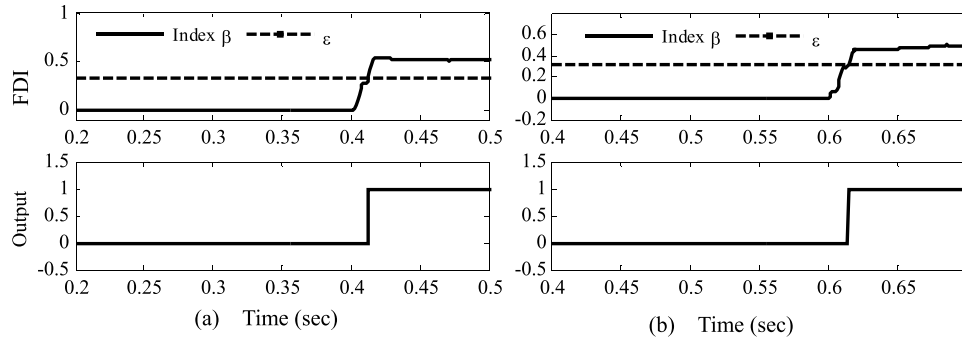
Fig. 9. Results for LG faults. (a) AG-faults. (b) CG-faults.

4.7. Response during varying fault resistance

The fault resistance is varied in the range of 5Ω to 100Ω and response of the method is tested. The fault inception time is 0.3 sec and fault location is 25 km. Different LG faults are created and computed values of FDI for individual fault cases are shown in Fig. 14. Due to increase in the fault resistance, differential positive sequence current value reduces but with this also the computed FDI values lie above the threshold. So, even with high fault resistance path also accurate detection of different faults is possible.

4.8. Impact of varying wind speed

The optimal threshold value is also tested against varying wind speed of wind farm within acceptable limits. AG faults with different fault locations are simulated for varying wind speed condition and results are demonstrated in Fig. 15. For $x = 5$ km from bus P, FDI is highlighted in red color and similarly black, blue and green colors are used to highlight the FDI plots for $x = 10$, 15 and 20 km. In Fig. 15 (a), the results are provided for increasing wind speed conditions and in Fig. 15 (b) results for decreasing order of wind speed are provided. In all test cases, fault incepted at 0.3 sec. and fault resistance is of 10 Ω. Results prove that under varying wind speed condition also the performance of the proposed method is accurate.

4.9. Impact of fault parameter on detection time

Fig 16 (a) show the response times of various unsymmetrical faults (AG, AB and ABG) during varying fault location condition. In Fig. 16 (b) the results for ABC fault cases are provided. For all cases, fault resistance of 5 Ω is considered. For AG fault initiation time is 0.3 sec and 0.35 sec for AB fault. In case of ABG and ABCG faults, initiation time is 0.4 sec. However, irrespective of type, location and initiation time, detection time is less and results are accurate.
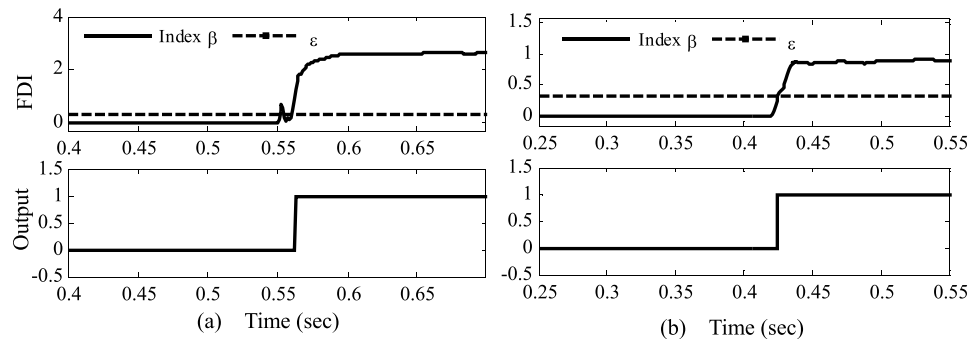
4.10. Response during dynamic operating conditions

The proposed intelligent threshold setting mechanism is further tested for dynamic operating conditions of the wind farm integrated power system. The variation of control parameters, wind speed and power variations are taking into consideration. It is to be noted that PSO assisted threshold setting mechanism is an off-line process because in practice dynamic operating of wind farm cannot be considered online to modify the threshold value. PSO assisted threshold setting equations are developed based on the variations of the control parameters using curve fitting technique. These equations can directly generate suitable threshold values based on the corresponding change in the test system without any computational burden on the relay. In this way, the practical implementation of the proposed scheme can be validated during different operating modes of the system. For this purpose, two control parameters known as DC bus voltage regulator (k_{pv}) and speed regulator (k_{ps}) are considered to develop direct PSO assisted threshold setting equations obtained by PSO curve fitting. Different optimal threshold values achieved through the PSO technique for various control parameters are computed and reported in Table 3–6.

The predicted optimal threshold values are achieved from the linear regression models developed by optimal threshold values achieved by using PSO technique. In Table 3, the DC bus voltage regulator is decreased from its operating value and thus the fitting equation can be written as

$$\vartheta = -0.0029k_{pv} + 0.3397 \tag{23}$$

With the help of Eq. (23), threshold values can be predicted for different voltage regulator values. The percentage of absolute error indicates that the optimal threshold value is nearly equal to the operating threshold value. Similarly, other equations can be obtained for DC regulator gains, and speed regulator gains as mentioned in Table 4–6 and can be represented as

$$\vartheta = 0.000299k_{pv} + 0.3148 \tag{24}$$

$$\vartheta = -0.0092k_{ps} + 0.3419 \tag{25}$$

Fig. 10. Results for double-line faults. (a) BC-faults. (b) ACG-faults.
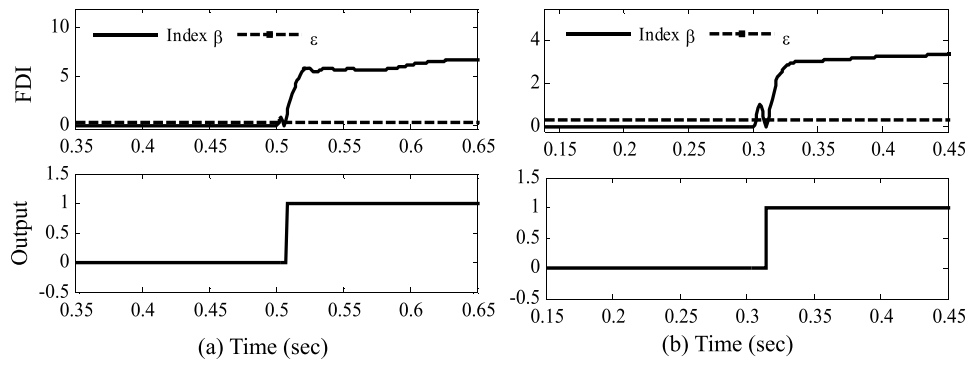
Fig. 11. Results for Symmetrical faults. (a) ABC-faults. (b) ABCG-faults.
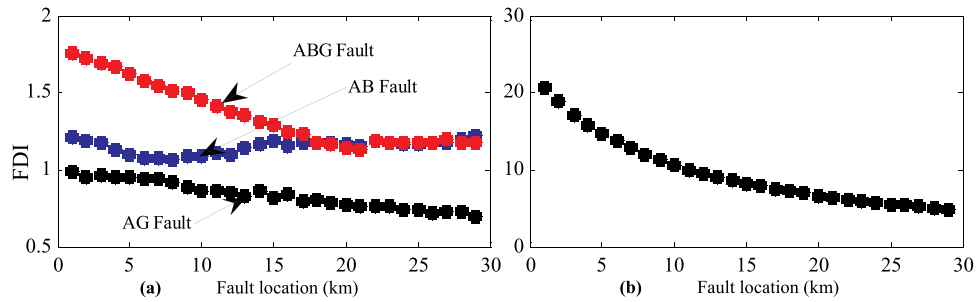
Fig. 12. Results for different fault location at fault resistance = 10Ω and t_s = 0.3 sec. (a) AG, AB, ABG faults. (b) ABCG faults.
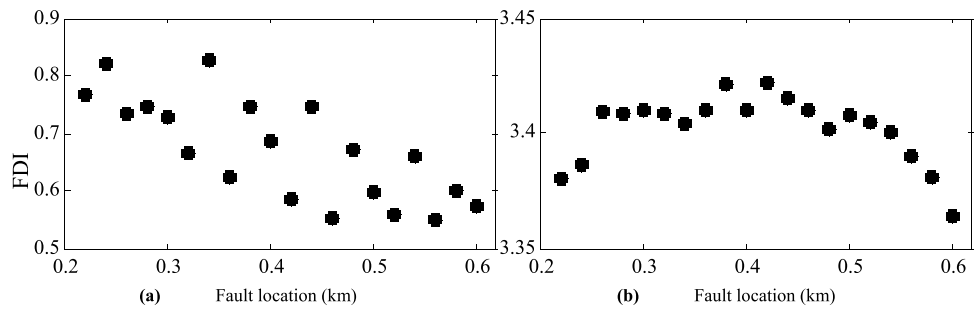
Fig. 13. Results for different fault location at fault resistance = 10Ω and t_s = 0.3 sec. (a) BG faults. (b) ABCG faults.
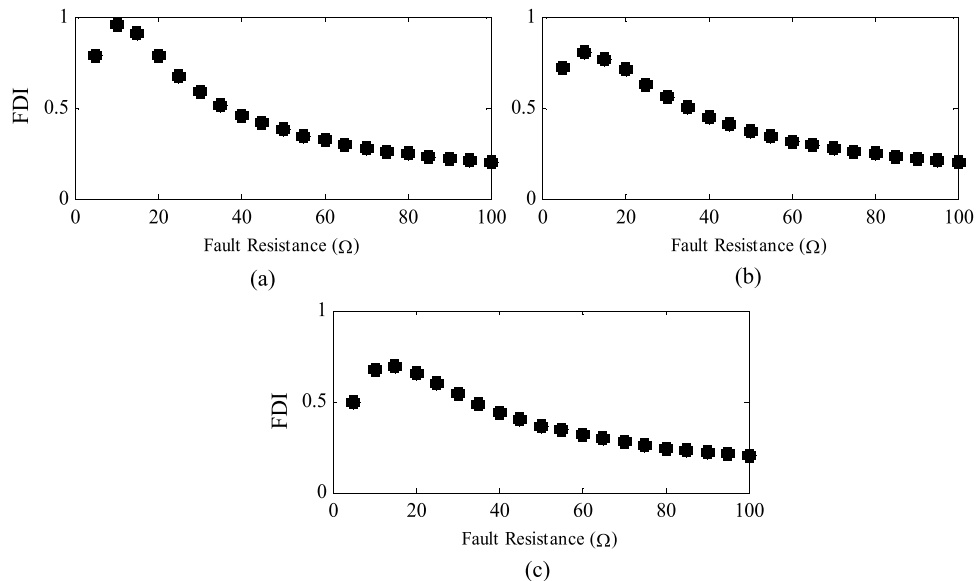
Fig. 14. Results for different fault resistances with t_s = 0.3 sec and x = 25 km. (a) AG faults. (b) BG faults. (c) CG faults.
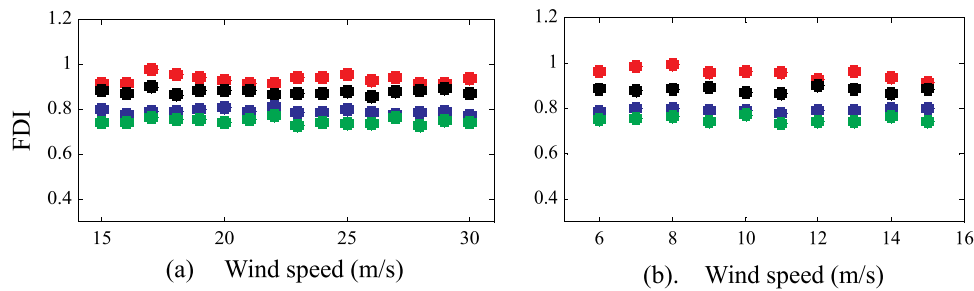
Fig. 15. Impact of variation in wind speed. (a) Increasing order. (b) Decreasing order.
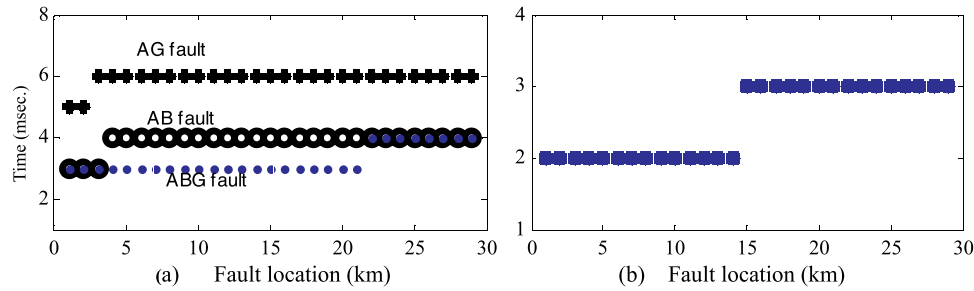
Fig. 16. Response time during varying fault parameters. (a) AG, AB, ABG faults. (b) ABC faults.

Table 3
Optimal threshold values for different DC regulator gains.

k_{pv}	Fault location by PSO (km)	Inception time by PSO (s)	Optimal threshold by PSO	Predicted Optimal threshold	Absolute Error in %
0.8	17.8774	0.4045	0.3341	0.3374	0.9817
4	20.9475	0.4128	0.3339	0.3281	1.7370
8	18.9150	0.4044	0.3137	0.3165	0.8926

Table 4
Optimal threshold values for different DC regulator gains.

k_{pv}	Fault location by PSO (km)	Inception time by PSO (s)	Optimal threshold by PSO	Predicted Optimal threshold	Absolute Error in %
8	18.9150	0.4044	0.3137	0.3172	1.1120
20	26.0564	0.4047	0.3256	0.3208	1.4830
40	19.8190	0.4127	0.3259	0.3267	0.2585
80	24.6125	0.4043	0.3383	0.3387	0.1137

Table 6
Optimal threshold values for different speed regulator gains.

k_{ps}	Fault location by PSO (km)	Inception time by PSO (s)	Optimal threshold by PSO	Predicted Optimal threshold	Absolute Error in %
3	18.9150	0.4044	0.3137	0.3195	1.8379
10	23.2504	0.4127	0.3296	0.3229	2.0374
20	25.3704	0.4045	0.3298	0.3278	0.6156
30	16.8376	0.4130	0.3296	0.3327	0.9267

$$\vartheta = 0.000488 k_{ps} + 0.3180 \tag{26}$$

Once these equations are available, then the threshold values can be automatically adjusted based on the dynamic conditions of the system and hence reliable protection operation can be ensured.

4.11. Influence of sampling frequency

The influence of the change in sampling frequency on the threshold setting mechanism is tested and discussed in this section. To conduct the test, different LG faults are created by varying the fault parameters. Results are reported in Table 7. The objective function of the proposed

intelligent threshold setting scheme is designed based on the maximum peak value of the differential positive sequence current component and therefore the change in sampling frequency effect is negligible on the overall performance of the scheme, which can be observed from Table 7.

4.12. Impact of variation in wind power

Wind power varies dynamically and due to this the operation of preset threshold based protective relay may face challenges. In order to test the response of the proposed method under such a condition, an unsymmetrical fault during varying wind power condition is simulated.

Table 5
Optimal threshold values for different speed regulator gains.

k_{ps}	Fault location by PSO (km)	Inception time by PSO (s)	Optimal threshold by PSO	Predicted Optimal threshold	Absolute Error in %
0.3	20.2755	0.4128	0.3383	0.3391	0.2483
1.5	17.6800	0.4128	0.3338	0.3281	1.7076
3	18.9150	0.4044	0.3137	0.3143	0.1913

Table 7
FDI for different sampling frequencies.

Fault	Fault location (km)	Fault inception time (s)	Fault resistance (Ω)	Sampling frequency				
				0.3 kHz	0.6 kHz	1.2 kHz	2.4 kHz	6 kHz
AG	12	0.406	20	0.6892	0.6893	0.6901	0.6778	0.6807
BG	08	0.415	30	0.5604	0.5603	0.5607	0.5643	0.5652
CG	18	0.411	45	0.3967	0.3967	0.3967	0.3960	0.3983
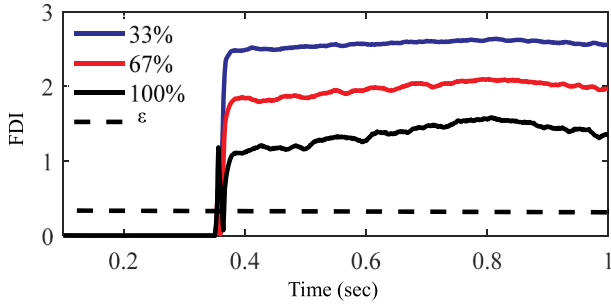
Fig. 17. Results for varying wind power penetration level.

Table 8
HIF model parameters.

Cases	Vp (kV)	Vn (kV)	Rp (Ω)	Rn (Ω)
Case-I	0.24 ± 4.2%	0.23 ± 2.2%	15~25	15~25
Case-II	0.24 ± 4.2%	0.23 ± 2.2%	100 ~150	100~150
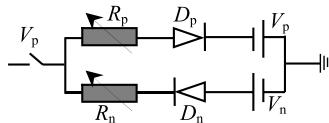
Fig. 18. High impedance fault model.

ABG fault with fault resistance of 20 Ω is created at 0.35 sec. The fault location is 18 km from bus-P. Three cases of 33%, 67% and 100% wind power penetration levels are investigated considering the ABG fault condition. The obtained results are depicted in Fig. 17. It is to be noted that, the optimal threshold value in the proposed work is designed for 100% wind power penetration level. Hence, the impact of variation in the wind power has negligible impact on the response of the proposed method which can be observed from Fig. 17.
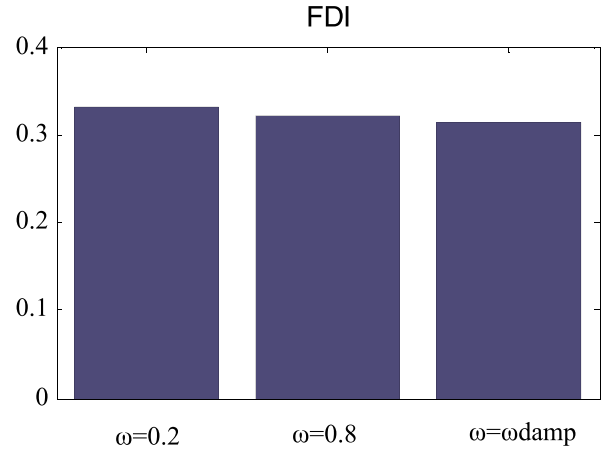
Fig. 20. FDI values obtained by PSO at different inertia weights.

Table 9
Comparison of optimal FDI's for various inertia weights of PSO.

Inertia weight case	Fault location	Fault inception	Optimal FDI
0.2	20.9246	0.4132	0.3319
0.8	18.5949	0.4045	0.3220
Proposed	18.9150	0.4044	0.3137

5. Comparative assessments and discussion

For comparative analysis the existing threshold selection approach as reported in [12] is considered and responses of both proposed and existing methods are verified for high impedance and low impedance fault cases.

5.1. High impedance faults

The high impedance faults often occur in distribution network and the condition may develop if the path will be a high impedance surface
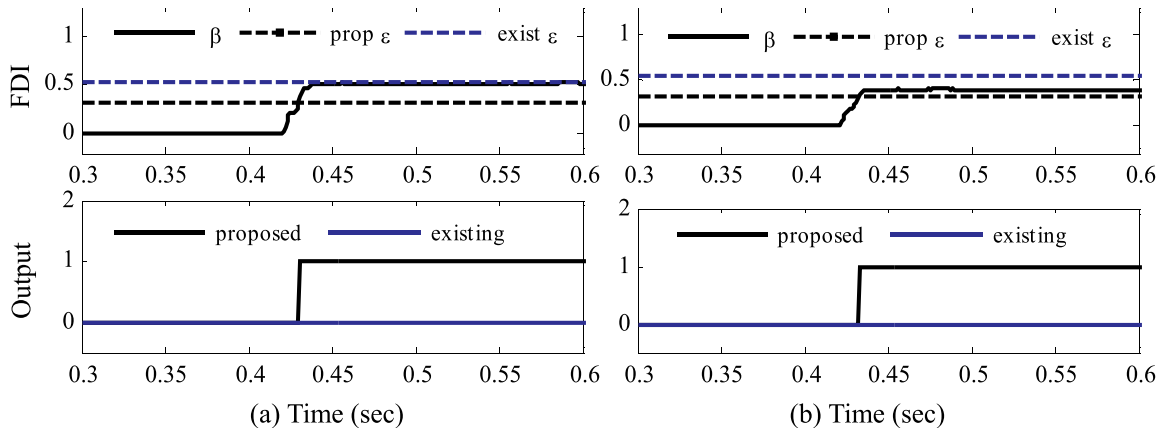
Fig. 19. Comparative analysis results for high impedance fault cases. (a) Case-I and (b). Case-II.

such as concrete, tree, or asphalt. The fault possesses nonlinear characteristics and the fault current may be in the order of normal load current, which makes the relay unable to take accurate decision [26]. In order to investigate the response of the method for such a condition, two different fault cases are simulated and the details of high impedance fault parameters are provided in Table 8. The high impedance fault model as shown in Fig. 18 is used and simulated using MATLAB R2016a software. The fault is created in between bus P and W.

In Case-I, the fault detection index is computed using conventional positive sequence current differential scheme. Then through the selected threshold based on proposed method and existing method are checked against the detection of the fault. From Fig. 19 (a) it can be observed that the FDI lies below the threshold selected using existing technique and consistently lie above the optimal threshold selected using proposed technique. For Case-II shown in Fig. 19 (b), the optimal threshold is working correctly. So, the threshold selected based on trial and error method cannot be reliable always. But the optimal threshold will be more effective in detecting fault in power network.

5.2. Discussion

As mentioned in Section 3, the application of PSO provides optimal threshold which is able to detect all possible faults in transmission lines. The proposed algorithm is a population search-based technique which initializes the process with random solutions. So, for the identification of the optimal threshold values, multiple executions are required so as to eliminate the pre-maturity condition of PSO and to achieve best minimum value (global optimum) through the objective function. On the other hand, selection of control parameters will also influence the convergence of the technique to achieve global optimum solution of the problem especially inertia weight factor. Instead of taking existing inertia weight strategies [23], a simple dynamic inertia concept is used in this paper to update the inertia weight for next iterations towards global optimum solution. The optimal threshold of 0.3137 is identified at 18.915 km from bus P during AG fault using the proposed PSO. The obtained FDI value is compared with the constant inertia weight based PSO assisted values and the results are presented in Fig. 20. The obtained optimal indices achieved through PSO solution for different fault locations and inception time are provided in Table 9. From the cases

mentioned in Table 9, it is clear that identification of optimal threshold is difficult by conventional approaches because every case produces different solution close to actual solution. But by using proposed method minimum FDI can be achieved. In this process, control and common parameters are maintained as same for different inertia weights. The threshold setting mechanism is important in relaying for the secure and reliable operation of fault detection and the proposed PSO yields better threshold compared to conventional mechanisms.

From the comparative results it is observed that, the proposed PSO yields better solution than conventional PSO. This proves the efficacy of the proposed method as compared to conventional PSO and existing approaches in detecting fault when applied to a wind farm integrated power network.

6. Conclusions

In this paper, an innovative threshold selection process is presented for differential protection algorithm applied to wind farm penetrated power network. The method uses swarm intelligence technique. The conventional differential scheme suffers from threshold setting problem especially in presence of dynamic operating conditions of power system due to integration of wind farms. To mitigate this, PSO assistance is provided to the differential protection scheme so that overall reliability can be improved. Under dynamic operating conditions of wind farm, the response of the method is accurate. The most accurate minimum threshold identified through PSO gives high reliability and it cannot be achieved through conventional trial and error method of threshold setting. The computational burden by the proposed approach is negligible as compared to existing relay schemes. The threshold setting process is based on off-line calculation, and hence even with the dynamic operating conditions of wind farm the speed and reliability of operation will not be compromised.

Declaration of competing interest

The authors declare that they have no known competing financial interests or personal relationships that could have appeared to influence the work reported in this paper.

Appendix

Component	Specifications
Transformer (T1)	1975/575 V, 1.5/0.9 MVA, magnetizing inductance $= 2.9$ p.u.
Transformer (T2)	575 V/25 kV, 1.75 $\times$ 6 MVA, $R_1 = R_2 = 0.00083$ p.u, $L_1 = L_2 = 0.025$ p.u, $R_m = L_m = 500$ p.u
Transformer (T3)	25/120 kV, 47 MVA, $R_1 = R_2 = 0.00267$ p.u, $L_1 = L_2 = 0.08$ p.u, $R_m = L_m = 500$ p.u
Grounding Transformer	25 kV, 100MVA and $R_0 = 0.25$, $X_0 = 0.75$ p.u
Line Filter	$C = 120$ kvar, $Q = 50$
Choke	$R = 0.003$ and $L = 0.3$ p.u
Source (Grid side)	$Vs = 120$ kV $Z_{1s} = 0.576 + j5.76$ O, $Z_{0s} = 1.728 + j17.28$ Ω
Line parameters	$Z_{1L} = 0.0201 + j0.2868$ Ω/km and $Z_{0L} = 0.1065 + j0.8671$ Ω/km

References

[1] PB Erikson, et al., System operation with high wind generation, IEEE Power Energy Mag. 3 (6) (2005) 65–74.

[2] Z Chen, Wind power in modern power systems, J. Modern Power Syst. Clean Energy 1 (1) (2013) 2–13.

[3] SP Chowdhury, S Chowdhury, PA Crossley, Islanding protection of active distribution networks with renewable distributed generators: a comprehensive survey, Electric Power Syst. Res. 79 (6) (2009) 984–992.

[4] R Nale, M Biswal, AY Abdelaziz, Protection Schemes for Sustainable Microgrids, Sustainable Interdependent Networks: From Theory to Application, Springer, 2018, pp. 267–296.

[5] AA Memon, K Kauhaniemi, A critical review of AC microgrid protection issues and available solutions, Electric Power Syst. Res. 129 (2015) 23–31.

[6] E Orduna, F Garces, E Handschin, Algorithmic-knowledge-based adaptive coordination in transmission protection, IEEE Trans Power Del. 18 (2003) 61–65.

[7] AK Pradhan, G Joos, Adaptive distance relay setting for lines connecting wind farms, IEEE Trans. Energy Conv. 22 (2007) 206–213.

[8] H Sadeghi, A novel method for adaptive distance protection of transmission line connected to wind farms, Int. J. Electr Power Energy Syst. 43 (1) (2012) 1376–1382.

[9] MA Haj-Ahmed, MS Illindala, Intelligent coordinated adaptive distance relaying, Electric Power Syst. Res. 110 (2014) 163–171.

[10] J Ma, W Zhang, J Liu, JS Thorp, A novel adaptive distance protection scheme for DFIG wind farm collector lines, Int. J. Electrical Power Energy Syst. 94 (1) (2018) 234–244.

[11] A Hooshyar, MA Azzouz, EF El-Saadany, Distance protection of lines connected to induction generator-based wind farms during balanced faults, IEEE Trans. Sustain. Energy 5 (4) (2014) 1193–1203.

[12] G. Yang, et al., The influences and countermeasures of wind farm access to transmission line differential protection, Proc. IEEE Conf. Power Electron. Mach. Wind

Appl, 2012, pp. 1–4.

[13] S Dambhare, SA Soman, MC Chandorkar, Adaptive current differential protection schemes for transmission-line protection, IEEE Trans. Power Del. 24 (4) (2009) 1832–1841.

[14] MA Zamani, TS Sidhu, A Yazdani, A communication-based strategy for protection of microgrids with looped configuration, Electric Power Syst. Res. 104 (2013) 52–61.

[15] TA Kawady, AM Taalab, ES Ahmed, Dynamic performance of the power differential relay for transmission line protection, Int. J. Electrical Power Energy Syst. 32 (5) (2010) 390–397.

[16] M Wen, D Chen, X Yin, An energy differential relay for long transmission lines, Int. J. Electrical Power Energy Syst. 55 (2014) 497–502.

[17] MK Jena, SR Samantaray, L Tripathy, Decision tree-induced fuzzy rule-based differential relaying for transmission line including unified power flow controller and wind-farms, IET Gener. Transm. Distrib. 8 (12) (2014) 2144–2152.

[18] S Biswal, M Biswal, OP Malik, Hilbert huang transform based online differential relay algorithm for shunt compensated transmission line, IEEE Trans. Power Del. 33 (6) (2018) 2803–2811.

[19] OA Gashteroodkhani, M Majidi, M Etezadi-Amoli, A combined deep belief network and time-time transform based intelligent protection Scheme for microgrids, Electric Power Syst. Res. 182 (2020) 106239.

[20] A Ghorbani, H Mehrjerdi, NA Al-Emadi, Distance-differential protection of

transmission lines connected to wind farms, Int. J. Electrical Power Energy Syst. 89 (2017) 11–18.

[21] Y Del Valle, GK Venayagamoorthy, S Mohagheghi, JC Hernandez, RG Harley, Particle swarm optimization: basic concepts, variants and applications in power systems, IEEE Trans. Evol. Comput. 12 (2) (2008) 171–195.

[22] MR AlRashidi, ME El-Hawary, A survey of particle swarm optimization applications in electric power systems, IEEE Trans Evol. Comput. 13 (4) (2009) 913–918.

[23] JC Bansal, PK Singh, Mukesh Saraswat, Abhishek Verma, Shimpi Singh Jadon, Ajith Abraham, Inertia weight strategies in particle swarm optimization, 2011 Third world congress on nature and biologically inspired computing, 2011, pp. 633–640.

[24] CD Prasad, PK Nayak, Performance assessment of swarm-assisted mean error estimation-based fault detection technique for transmission line protection, Comput. Electr. Eng. 71 (2018) 115–128.

[25] CD Prasad, M Biswal, PK Nayak, Wavelet operated single index based fault detection scheme for transmission line protection with swarm intelligent support. Energy systems, Springer, 2020, https://doi.org/10.1007/s12667-019-00373-9.

[26] X Wang, J Gao, X Wei, G Song, Lei Wu, J Liu, Z Zeng, M kheshti, High impedance fault detection method based on variational mode decomposition and Teager-Kaiser energy operators for distribution network. 2008) Particle swarm optimization: basic concepts, variants and applications in power systems, IEEE Trans. Smart Grid 10 (6) (2019) 6041–6054.